LIQUID DIELECTRIC FILMS IN A NONUNIFORM ELECTRIC FIELD: DYNAMICS, PERFORATION, AND INFLUENCE OF ELECTRODE WETTABILITY

*D.A. Medvedev & A.L. Kupershtokh**

Lavrentyev Institute of Hydrodynamics, Siberian Branch of Russian Academy of Sciences, 15, Lavrentyeva Prosp., Novosibirsk, 630090, Russia

*Address all correspondence to: A.L. Kupershtokh, Lavrentyev Institute of Hydrodynamics, Siberian Branch of Russian Academy of Sciences, 15, Lavrentyeva Prosp., Novosibirsk, 630090, Russia; Tel.: +7 383 333 3249; Fax: +7 383 333 1612, E-mail: sknew@mail.ru

A nonstationary electrohydrodynamic model of dielectric film dynamics on a solid substrate in surrounding gas is developed. The mesoscopic multiphase lattice Boltzmann model is applied for simulation of fluid dynamics. The nonuniform electric field is generated by inserting nonconductive parts into the lower electrode. Under the action of a nonuniform electric field, the film can be perforated producing new contact lines. In the case of a round insulating inset, the perforation process is governed by the electric field strength, the film thickness, the radius of nonconductive insets, and the contact angle between the liquid and the solid substrate. Hence the modified expression for the electric Bond number can be introduced, which takes into account both the film thickness and the radius of nonconductive insets. When the inset radius is substantially larger than the thickness of a film, the wetting of the electrode does not play an essential role in the initial perforation but influences the dynamics of the dry spot growth. When the size of the insulating parts is comparable with the film thickness, the situation becomes different. With certain electric field strength, the film is teared faster on a nonwettable surface of inserts but can be preserved on a wettable one. It was shown that the degree of wetting of insulating insets makes the main difference.

KEY WORDS: *dielectric liquid, electric field, liquid films, computer simulations, graphics processing unit, lattice Boltzmann method*

1. INTRODUCTION

The effective cooling of hot surfaces is very important in microfluidic and microelectronic devices. One of the methods for cooling is the creation of thin films or many droplets of evaporating liquid placed onto a solid surface with three-phase contact lines (Potash and Wayner, 1972; Wayner, 1989). It was shown theoretically and in experiments that the main heat flux occurs near the contact lines (Karchevsky et al., 2016; Ajaev and Kabov, 2017). Thus, in order to increase the cooling efficiency, it is promising to create new contact lines by perforating liquid films.

Many studies, experimental, theoretical, and with computer simulations, are devoted to the behavior of droplets (Taylor, 1964; Imano and Beroual, 2006; Liu et al., 2008; Vancauwenberghe et al., 2013; Corson et al., 2014, 2016; Gibbons et al., 2016; Akbari and Mortazavi, 2017; Medvedev and Kupershtokh, 2021), bubbles (Korobeynikov et al., 2019; Wang et al., 2017; Kupershtokh and Medvedev, 2019), and liquid films (Medvedev and Kupershtokh, 2021; Zubarev, 2002) under the action of an electric field. The electric field was also used to manipulate the droplets (Liu et al., 2008; Medvedev and Kupershtokh, 2021). The action of an electric field on dielectric droplets can also enhance heat transfer from a solid substrate (Vancauwenberghe et al., 2013). However, there are no numerical studies of the perforation of dielectric films in an electric field, except the work (Medvedev and Kupershtokh, 2021).

In Medvedev and Kupershtokh (2021), the possibility of the rupture of liquid films by the action of a nonuniform electric field was demonstrated. There the authors investigated numerically the process of generation of new contact

<div style="border:1px solid">

NOMENCLATURE

A	free parameter in the forcing scheme	w_k	weights in the equilibrium distribution functions
B	wettability parameter		
Bo	Bond number	**Greek Symbols**	
Bo_E	electric Bond number	α	polarizability in the Clausius–Mossotti formula
Bo_E^*	modified electric Bond number	β	contact angle
$\mathbf{c}_k$	velocities of pseudoparticles	δ	initial film thickness
E	electric field	ε	electric permittivity
f_k	distribution functions for lattice Boltzmann method	ε_0	electrostatic constant
f_k^{eq}	equilibrium distribution functions	θ	kinetic temperature
		ν	kinematic viscosity
$\mathbf{F}$	force acting on fluid	ρ	fluid density
h	lattice spacing	σ	surface tension
l_S	width of strips	τ	nondimensional relaxation time
P	fluid pressure	ϕ	electric potential
R_{in}	radius of nonconductive inset	Φ	special function in the forcing scheme
T	fluid temperature	Ω	collision operator
t	time		
$\mathbf{u}$	fluid velocity	**Subscripts**	
U	pseudopotential	cr	critical values
V	voltage between electrodes	l	liquid
g	gravity acceleration	x,y,z	spatial directions

</div>

lines by perforating liquid dielectric films. The nonuniform field was produced at the boundaries of nonconductive insets in a lower electrode. This electrode was electrically grounded. When a high voltage was applied to an upper flat electrode, the dielectric liquid was pulled into the regions of increased magnitude of the electric field. In this case, depending on the geometry and the field strength, the rupture of the film and, consequently, the appearance of new contact lines may occur.

In the present work we perform further studies of the perforation of a liquid film by a nonuniform electric field. We study the influence of the different values of wettability of nonconductive insets that plays a decisive role in this process. We also demonstrate in the present work the perforation process for an array of round insets. Three-dimensional computer simulations of this process are carried out. The dimensionless parameters governing the film's behavior are the Bond number and the electric Bond number.

The lattice Boltzmann equation method (LBE, LBM) is used for simulations of these nonstationary two-phase fluid dynamics (McNamara and Zanetti, 1988; Shan and Chen, 1993; Kupershtokh et al., 2009; Kupershtokh, 2010; Kupershtokh and Medvedev, 2018). It was first applied to simulate electrohydrodynamic flows in Medvedev and Kupershtokh (2000) and Kupershtokh and Medvedev (2006). This method takes into account the surface tension at the liquid-vapor interface, the gravitational and electrostatic forces, and also the interaction of fluid with solid substrate. The electrical and hydrodynamic equations of the three-dimensional problem are solved jointly. The distribution of the electric field strength in the entire region between flat electrodes is calculated numerically at each time step by solving the Poisson's equation for the potential of the electric field.

The CUDA (Compute Unified Device Architecture) technology is used for parallel programming on GPU. In Section 2 we briefly describe the multiphase lattice Boltzmann method for simulating the fluid dynamics and the details of the solution of Poisson's equation and the calculation of electric forces with corresponding boundary conditions. Section 3 is devoted to the investigation of the penetration of liquid films at electrodes with round insulating insets. In Section 4, the dynamics of dielectric films at electrodes with alternating conductive and nonconductive stripes is simulated. Section 5 gives some concluding remarks.

2. NUMERICAL METHOD

2.1 Lattice Boltzmann Method

The lattice Boltzmann method simulates the fluid flows as the dynamics of an ensemble of pseudoparticles that can move along the links of the regular spatial lattice. Only the limited set of the velocities of the pseudoparticles $\mathbf{c}_k$ is used. In the 19-speed LB model D3Q19 (Qian et al., 1992) used in this work, the possible values of $|\mathbf{c}_k|$ are 0, $h/\Delta t$, and $\sqrt{2}h/\Delta t$ (h is the lattice spacing, Δt is the time step). Corresponding lattice vectors are $\mathbf{e}_k = \mathbf{c}_k \Delta t$. The one-particle distribution functions f_k evolve according to the equation

$$f_k(\mathbf{x} + \mathbf{c}_k \Delta t, t + \Delta t) = f_k(\mathbf{x}, t) + \Omega_k\{f_k\} + \Delta f_k. \tag{1}$$

The collision operator Ω_k is taken in the form of the relaxation to local equilibrium with a single relaxation time (the BGK form [Qian et al., 1992])

$$\Omega_k(f_k(\mathbf{x}, t)) = \frac{f_k^{eq}(\rho, \mathbf{u}) - f_k(\mathbf{x}, t)}{\tau}. \tag{2}$$

The dimensionless relaxation time τ determines the kinematic viscosity of fluid $\nu = (\tau - 1/2)\theta\Delta t$. Here, $\theta = (h/\Delta t)^2/3$ is the kinetic temperature of LBE pseudoparticles. The equilibrium distribution functions f_k^{eq} are usually taken in the form of truncated Maxwellians (Koelman, 1991)

$$f_k^{eq}(\rho, \mathbf{u}) = \rho w_k \left(1 + \frac{(\mathbf{c}_k \cdot \mathbf{u})}{\theta} + \frac{(\mathbf{c}_k \cdot \mathbf{u})^2}{2\theta^2} - \frac{\mathbf{u}^2}{2\theta} \right). \tag{3}$$

The density ρ and the mass velocity of the fluid $\mathbf{u}$ are calculated as the first two moments of the distribution functions f_k

$$\rho = \sum_{k=0}^{18} f_k \quad \text{and} \quad \rho\mathbf{u} = \sum_{k=1}^{18} \mathbf{c}_k f_k.$$

The weight coefficients for the D3Q19 model are $w_0 = 1/3$, $w_{1-6} = 1/18$, and $w_{7-18} = 1/36$ (Qian et al., 1992).

We use the exact difference method (EDM) (Kupershtokh, 2004, 2010) for Δf_k to take into account the body forces (internal, gravitational, and electrostatic)

$$\Delta f_k = f_k^{eq}(\rho, \mathbf{u} + \Delta\mathbf{u}) - f_k^{eq}(\rho, \mathbf{u}). \tag{4}$$

Here, $\Delta\mathbf{u} = \mathbf{F}\Delta t/\rho$ is the change in velocity during the time step due to body forces.

To simulate the phase transition, the internal forces between neighbor nodes of fluid are introduced. The total force acting on a node is expressed as the gradient of the pseudopotential $U = P(\rho, T) - \rho\theta$ (Qian and Chen, 1997)

$$\mathbf{F}_{int}(\mathbf{x}) = -\nabla U, \tag{5}$$

where $P(\rho, T)$ is the pressure calculated from the equation of state of fluid, and T is the temperature. We proposed earlier to introduce a special function $\Phi = \sqrt{-U}$ and to rewrite the formula (5) for the total force in the equivalent form (Kupershtokh, 2005; Kupershtokh et al., 2009, 2015; Kupershtokh and Medvedev, 2018)

$$\mathbf{F}(\mathbf{x}) = 2A\nabla(\Phi^2) + (1 - 2A)2\Phi\nabla\Phi. \tag{6}$$

Here, A is a free parameter that can be adjusted so that the coexistence curve corresponds best to the given equation of state of the fluid. For the van der Waals equation of state in reduced variables (density, temperature, and pressure), the value is $A = -0.152$ (Kupershtokh et al., 2009; Kupershtokh and Medvedev, 2018; Kupershtokh, 2005). Equation (6) allows one to write the approximation of the gradient of pseudopotential in a combined finite-difference form with improved isotropy (Kupershtokh et al., 2009, 2015; Kupershtokh, 2005; Kupershtokh and Medvedev, 2018). The surface tension is produced at the boundary between phases. Its value is equal to σ = 5.1 in lattice units for the reduced temperature $T/T_{cr} = 0.6$.

The wettability of the solid surface can be changed under the action of the electric field (Bateni et al., 2005). The lattice Boltzmann method includes this feature (electrowetting) as an intrinsic property. However, this effect is weak for the considered problem (Kupershtokh, 2020).

2.2 Geometry and Boundary Conditions

The calculations are performed in a rectangular domain with dimensions of L_x, L_y, L_z. The periodic boundary conditions are used in the x and y directions. We use the well-known "bounce-back" rule to simulate the no-slip boundary conditions at the flat electrodes at $z = 0$ and $z = L_z$ in the LBM simulations.

We use the model of wettability that introduces in LBM the interaction forces between a node $\mathbf{x}$ of fluid and the nearest five nodes on the solid wall (Kupershtokh, 2020)

$$\mathbf{F}(\mathbf{x}) = B\Phi(\mathbf{x}) \sum_{j=1}^{5} w(\mathbf{e}_j) \Phi_{\text{solid}}(\mathbf{x} + \mathbf{e}_j) \cdot \mathbf{e}_j. \tag{7}$$

Here, the value of the function Φ_{solid} takes the same value as one in the nearest node of fluid $\mathbf{x}$ located directly over this node of solid surface. Lattice vectors $\mathbf{e}_j$ point from a fluid node to these five wall nodes. The wettability of the solid surface is related to the parameter B (Kupershtokh, 2020). The value of contact angle β = 90° (neutral wettability) is obtained at $B = 1$. The values $B > 1$ correspond to the wetting case, and $B < 1$ to the nonwetting case.

2.3 Calculation of Electric Potential and Forces

The electrostatic force acting on a dielectric liquid without space charge is given by the Helmholtz formula (Landau and Lifshitz, 1959)

$$\mathbf{F} = -\frac{\varepsilon_0 E^2}{2}\nabla\varepsilon + \frac{\varepsilon_0}{2}\nabla\left[E^2\rho\left(\frac{\partial\varepsilon}{\partial\rho}\right)_T\right]. \tag{8}$$

Here, E is the local electric field magnitude, ε_0 is the electrostatic constant, and ε is the permittivity of fluid. For nonpolar dielectric fluids, the Clausius–Mossotti equation is used

$$\varepsilon = 1 + \frac{3\alpha\rho}{1 - \alpha\rho}. \tag{9}$$

Here the value of polarizability α is chosen to set the permittivity to a prescribed value ε_l for the reduced equilibrium density of liquid dielectric ρ_l used in simulations. The permittivity of vapor is close to unity. The dielectric permittivity $\varepsilon(\rho)$ of the fluid changes in space during the development of the process.

The calculations of electric field are carried out taking into account the changes of the permittivity distribution in space and, consequently, in time. The following equation for the distribution of the electric field potential φ between electrodes,

$$\nabla \cdot (\varepsilon_0\varepsilon \nabla\phi) = 0, \tag{10}$$

is solved at every time step using the well-known method of simple iterations (McDonough, 1985; Press et al., 1986), also known as the Jacobi method. For example, in the two-dimensional case with nonuniform permittivity the iteration step looks like

$$\hat{\phi}_{i,j} = \frac{\varepsilon_{i+1/2,j}\phi_{i+1,j} + \varepsilon_{i-1/2,j}\phi_{i-1,j} + \varepsilon_{i,j+1/2}\phi_{i,j+1} + \varepsilon_{i,j-1/2}\phi_{i,j-1}}{\varepsilon_{i+1/2,j} + \varepsilon_{i-1/2,j} + \varepsilon_{i,j+1/2} + \varepsilon_{i,j-1/2}}, \tag{11}$$

and can be easily extended for the three-dimensional case.

The periodic boundary conditions for the electric potential are used for side boundaries (along the x and y coordinates). The electric potential of the upper electrode is constant $\phi(x, y, L_z) = V$ (Fig. 1). The lower electrode is electrically grounded $\phi(x, y, 0) = 0$. At the surface of the nonconductive insets in the lower electrode we use the boundary conditions $\partial\phi/\partial z = 0$. After solving Eq. (10), the electric field is calculated as $\mathbf{E} = -\nabla\phi$.

To ensure the value of electric field E_0 over the initial surface of the film, the applied voltage should be equal to

$$V = E_0(L_z - \delta(1 - 1/\varepsilon_l)), \tag{12}$$

where δ is the initial thickness of the film.

3. PERFORATION OF LIQUID FILMS BY THE ELECTRIC FIELD

An example of modeling the perforation of a thin film in a nonuniform electric field is shown in Fig. 1. The round nonconductive inset of the radius R_{in} is located in the center of the dissected lower electrode. When a high voltage is applied, the dielectric liquid is pulled into the regions of increased electric field near the edges of the inset. In this case, depending on the thickness of the film, its rupture and, consequently, the appearance of a new contact line may occur (Fig. 1). Then the liquid continues to move not only due to electrostatic forces but also by inertia [Figs. 1(b) and 1(c)].

The dimensionless parameter that determines the behavior of a liquid droplet in a gravity field is the Bond number $\mathrm{Bo} = \rho g R^2/\sigma$, where σ is the surface tension, and R is the characteristic size of the droplet. For a liquid dielectric film, we can introduce the Bond number in the form $\mathrm{Bo} = \rho g \delta^2/\sigma$, where δ is the thickness of the film.

Obviously, the degree of deformation of a dielectric liquid increases with an increase in the electric field, but the situation with the electric Bond number for dielectric films is not simple. Our simulations show that the time until perforation also depends strongly on the size of the nonconductive insets R_{in} in the dissected electrode (Table 1), despite the fact that the electric Bond number $\mathrm{Bo}_E = 1.71$ does not change. This means that the usual definition $\mathrm{Bo}_E = \varepsilon_0(\varepsilon_l - 1)E_0^2\delta/(\varepsilon_l\sigma)$ is not correct, where E_0 is the value of electric field over the surface of the film. The values of the other parameters do not change: $\delta = 20$, $\varepsilon_l = 4$, $\sigma = 5.1$, $\tau = 0.58$, $B = 1$ (contact angle 90°). The lattice size is $560 \times 560 \times 144$.

At $R_{in} \geq 80$, we observe that the perforation of the film starts somewhat later than at $R_{in} = 60$ (Table 1). This can be explained by the fact that the rupture mechanism changes. In this case the rupture of the film begins not above
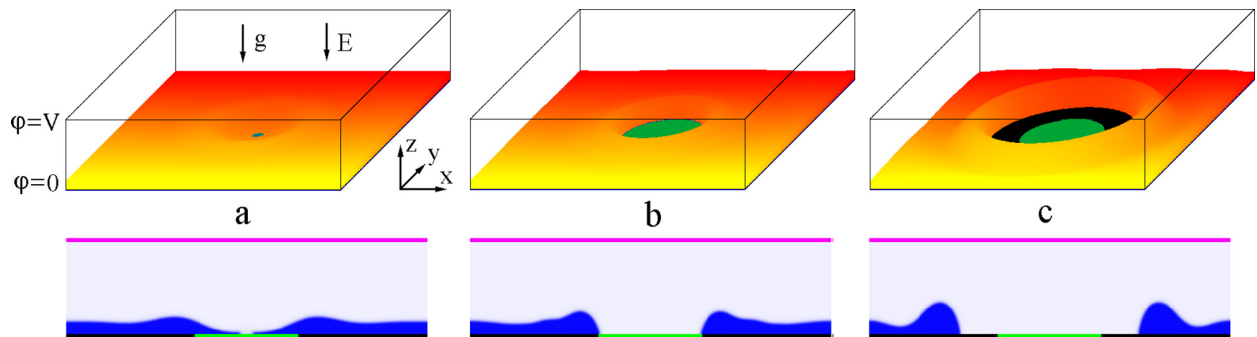
FIG. 1: Process of film perforation in an electric field. The lower row is density distributions of fluid in the central vertical cross section. The round nonconductive inset in the lower electrode is shown by the thick bar at the bottom. The parameters values are $\varepsilon_l = 4$, $\delta = 20$, $R_{in} = 80$, $\beta = 90°$, $\mathrm{Bo} = 0.018$, $\mathrm{Bo}_E = 1.18$, and $\mathrm{Bo}_E^* = 18.9$. Lattice size $560 \times 560 \times 144$. $t = 3900$ (a), 5500 (b), and 8600 (c).

TABLE 1: Time before perforation of liquid film at constant thickness of film

R_{in}	20	30	40	60	80	100
t	11,400	6700	4400	3200	3400	4000
Bo_E^*	1.71	3.84	6.82	15.3	27.3	42.6

the center of the inset but along a certain circumference, while the liquid droplet remains above the center of the inset (Fig. 2). As a result, the perforation process slows down.

On the other hand, we observe that the time to rupture unexpectedly increases with the film thickness at constant $R_{in} = 40$ (Table 2), despite the fact that the electric Bond number increases. Therefore, to take into account both the thickness of the film and the radius of inset, we propose to use in this case a modified definition of the dimensionless parameter

$$Bo_E^* = \varepsilon_0(\varepsilon_l - 1)E_0^2 R_{in}^2/(\delta\varepsilon_l\sigma). \tag{13}$$

This definition is more appropriate for evaluating the process of perforation of liquid dielectric films. With reasonable values of the parameters, e.g., $\delta = 2$ mm, $R_{in} = 8$ mm, $\varepsilon_l = 7$, and $\sigma = 0.073$ N/m, the value of the modified electric Bond number is $Bo_E^* = 3.33$ at the electric field strength of $E_0 = 10$ kV/cm. The breakdown electric field strength of typical dielectric liquids is higher than 100 kV/cm ($Bo_E^* > 300$, in this case). Regarding the surrounding gas over a liquid film, the breakdown electric field strength of air at atmospheric pressure is 30 kV/cm. However, the breakdown electric field strength of sulfur hexafluoride gas at normal pressure is three times higher than of air, that is, it is about 100 kV/cm. Moreover, the breakdown electric field strength of gases can be improved by increasing the pressure.
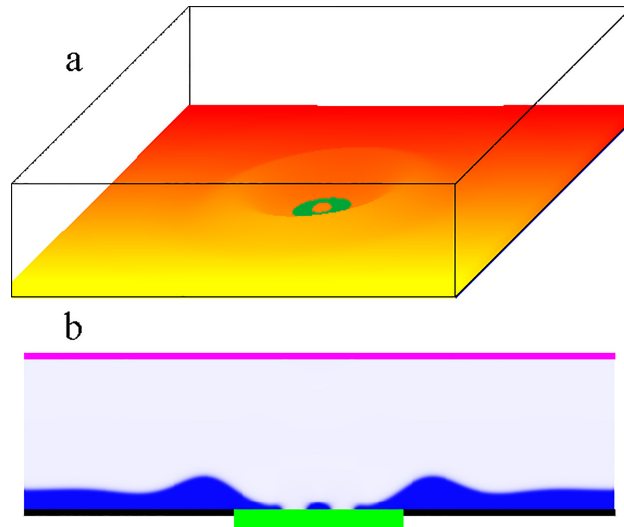
FIG. 2: (a) Process of film perforation with generation of a droplet. (b) Density distribution of fluid in the central vertical cross section. $t = 3400$. The round nonconductive inset in the lower electrode is shown by the thick bar at the bottom. Lattice size $560 \times 560 \times 144$. $\varepsilon_l = 4$, $\delta = 20$, $R_{in} = 80$, Bo = 0.018, $Bo_E = 1.71$, and $Bo_E^* = 27.3$.

TABLE 2: Time before perforation of liquid film at constant R_{in}

δ	20	30	40	50	60
t	4400	5800	7500	9400	11,000
Bo_E	1.71	2.56	3.41	4.27	5.12
Bo_E^*	6.82	4.55	3.41	2.73	2.27

The deformations of a thin film in an electric field lead to a local increase in the electric field. This increase in gas phase can be of order of $3\varepsilon_l/(\varepsilon_l + 2)$ times, and the magnitude of the electric field usually remains below the breakdown electric field strength.

The simulation of the process with four nonconductive round-shape insets is carried out. The insets are evenly distributed over the surface of the lower electrode, taking into account the periodic boundary conditions in x and y directions. The arrangement of the lower electrode with insets is shown in Fig. 3(a). The results of simulation are shown in Figs. 3(b) and 4. The parameter values are $\delta = 20$, $R_{in} = 60$, $\varepsilon_l = 4$, $\sigma = 5.1$, and $\text{Bo}_E^* = 12.9$.

The density distributions of fluid in the vertical cross section at the first row of insets for different values of contact angle are as follows (Fig. 4): $\beta = 90°$ (a), $60°$ (b), and $130°$ (c) for values $B = 1$, 1.06, and 0.92, respectively, in accordance with Kupershtokh (2020). One can see that the process of rupture of the liquid film begins later for a wettable surface ($60°$) and faster for a nonwettable one ($130°$) than for neutral wettability at $\beta = 90°$.

We also investigate the case of different wettabilities [Fig. 4(d)]: the contact angles are $\beta = 60°$ for the conductive part of the electrode and $\beta_{in} = 130°$ for the nonwettable insulating insets. Even with a well-wettable electrode in this case, the time before perforation of the liquid film is practically the same as for a completely nonwettable surface [Fig. 4(c)].

Parallel calculations are performed using all cores of GPU Titan-V (internal memory 12 Gb, 5120 cores). For the above-described three-dimensional LBE simulations of the dynamics of dielectric films in an electric field, the 3D lattices with sizes up to $560 \times 560 \times 144$ (45 million nodes) can be allocated in GPU internal memory. The performance of our calculations turned out to be over than 130 million node updates per second (MNUPS).

4. DYNAMICS OF FILMS ON A STRIPED ELECTRODE

We simulated the evolution of the liquid film placed initially at the lower electrode under the action of gravity and electric field. The lower electrode consists of alternating conductive and nonconductive strips of the same width. The initial height of the liquid dielectric layer is $\delta = 20$ lattice units, the size of the calculation domain was $320 \times 320 \times 101$, and the width of strips is $l_S = 40$. The gravity field is directed normal to the electrodes; its magnitude was $g_z = 8 \times 10^{-5}$ in lattice units, which corresponds to the Bond number $\text{Bo} = 0.015$.
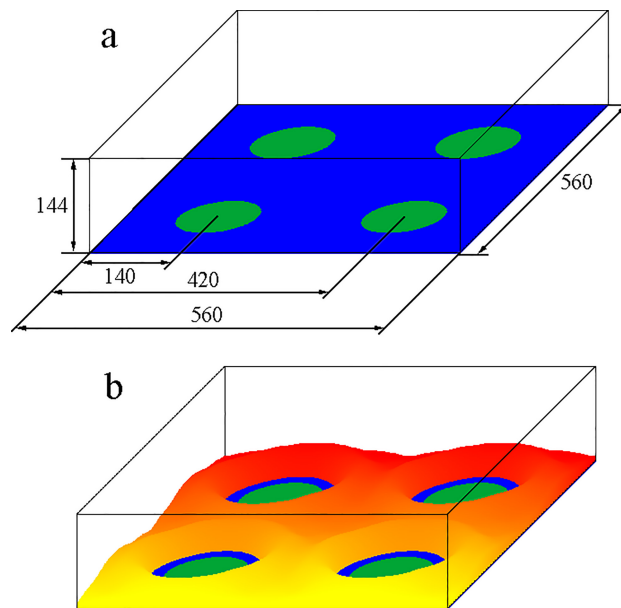
FIG. 3: (a) Arrangement of four nonconductive round-shape insets. (b) Process of film perforation in electric field. $t = 5600$. Lattice size $560 \times 560 \times 144$. $\beta = 90°$.
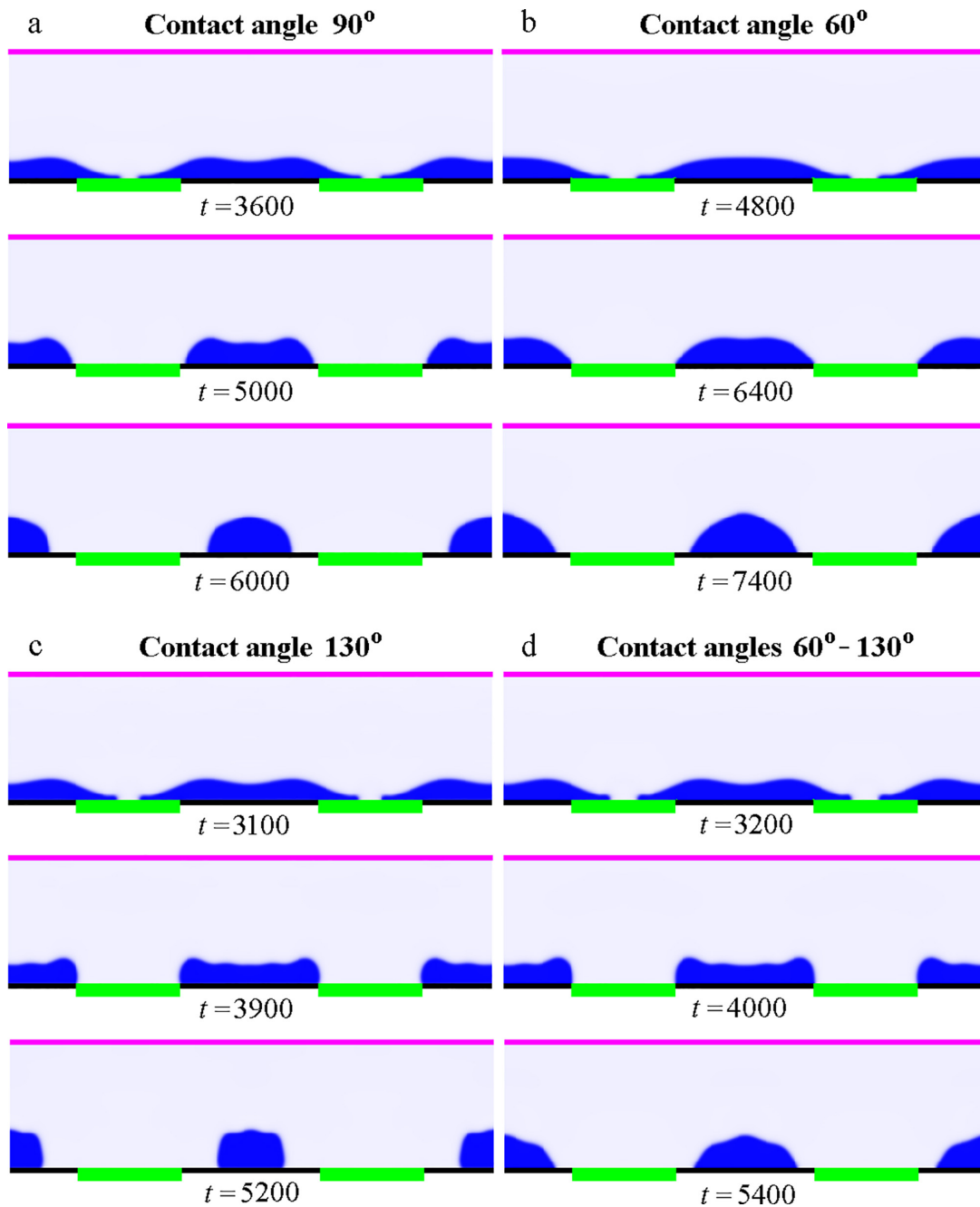
FIG. 4: Density distributions of fluid in vertical cross section at the first row of insets. Insets are shown by thick bars at the bottom. (a) $\beta = 90°$, (b) $\beta = 60°$ (wettable), (c) $\beta = 130°$ (nonwettable). (d) Different wettability: $\beta = 60°$ for the conductive part of the electrode and $\beta_{in} = 130°$ for the nonwettable insets.

Figure 5 shows the dynamics of a film for the same value of electric field corresponding to the electric Bond number $Bo_E = 0.614$ but different electrode wettability. For the upper row, the electrodes are nonwetting (contact angle $\beta = 70°$). In this case the film breaks up at the time $t \approx 1900$, the liquid ramparts are formed, and new triple-phase contact lines arise.

The lower row presents the results for wetting electrodes (the contact angle $\beta = 116°$). Here the initial deformation of the film is almost the same as in the previous case. However, the film does not break because of the higher value of the wetting energy.

On the contrary, in the next series of simulations, different wettability was assigned to the conductive and nonconductive parts of the lower electrode. The resulting film dynamics is shown in Fig. 6. For the upper row, the conductive parts of the electrode are separated by nonwettable insets (contact angles $\beta = 70°$ and $116°$, correspondingly). For the lower row, conductive strips were nonwettable ($\beta = 116°$) and nonconductive ones were wettable ($\beta = 70°$).

One can see that the dynamics of the liquid film at the same time points is quite similar to the case presented in Fig. 5, where wettability of the whole electrode was the same. Hence, the main conclusion is that only the wettability of the nonconductive stripes plays a decisive role. The reason for this is that after the application of voltage, the film gets thinner at nonconductive insets and here it "feels" the electrode surface. For thicker film at conductive stripes, the wetting of electrodes is not so significant.

5. CONCLUSIONS

We demonstrate the perforation of dielectric liquid films on a solid surface of electrode containing nonconductive insets as round or in the form of strips. At the constant magnitude of the electric field, the perforation time increases with the increase of the film thickness and decreases when the radius of the inset grows. The dimensionless parameter for estimation of time before perforation of dielectric films is the modified electric Bond number (13). However, with large radius of the inset, the rupture mechanism changes, and formation of a droplet or disk above the center of the inset is observed. On the wetting surface with smaller contact angle, the perforation process develops more slowly than on neutrally wetting ones.

When the lower electrode consists of conductive and nonconductive strips of the same width, the size of which is comparable with the initial film thickness, the qualitative effect of the surface wettability is observed. With certain electric field strengths, the film is teared faster on a nonwettable surface of insets, but a rupture can be prevented
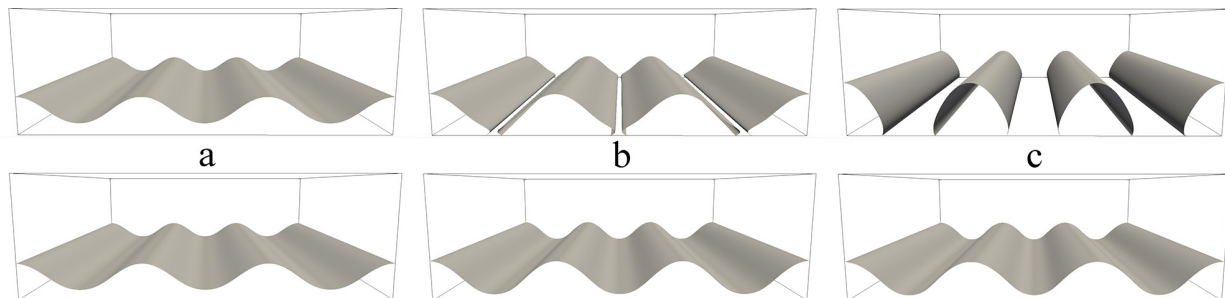
FIG. 5: Film deformation and breakup in nonuniform electric field. Upper row is for nonwettable lower plane surface and lower row is for the wettable one. Time $t = 1200$ (a), 1900 (b), and 3000 (c).
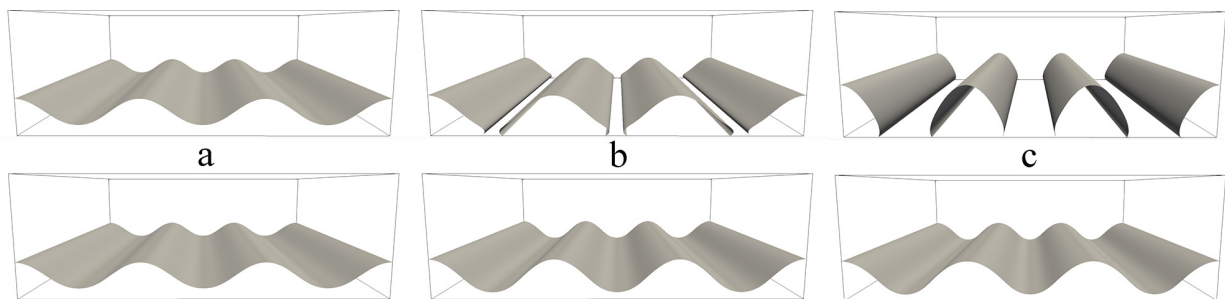
FIG. 6: Film deformation and breakup. Upper row is for nonwettable insulating insets and wettable conductive parts. Lower row is for wettable insets and nonwettable conductive parts. Time $t = 1200$ (a), 1900 (b), and 3000 (c).

on a wettable one. It was shown that the degree of wetting of insulating insets makes the main difference, whereas the wetting of conductive parts is not significant. Hence, changing the wettability of the electrode surface gives an additional degree of freedom for the control of the film perforation. The choice of optimal specific dielectric liquids and material of insets is a topic for a separate engineering study and is beyond the scope of this article.

ACKNOWLEDGMENT

REFERENCES

Ajaev, V.S. and Kabov, O.A., Heat and Mass Transfer near Contact Lines on Heated Surfaces, *Int. J. Heat Mass Transf.*, vol. **108**, pp. 918–932, 2017.

Akbari, M. and Mortazavi, S., Three-Dimensional Numerical Simulation of Deformation of a Single Drop under Uniform Electric Field, *J. Appl. Fluid Mech.*, vol. **10**, no. 2, pp. 693–702, 2017.

Bateni, A., Laughton, S., Tavana, H., Susnar, S.S., Amirfazli, A., and Neumann, A.W., Effect of Electric Fields on Contact Angle and Surface Tension of Drops, *J. Colloid Interf. Sci.*, vol. **283**, pp. 215–222, 2005.

Corson, L.T., Tsakonas, C., Duffy, B.R., Mottram, N.J., Sage, I.C., Brown, C.V., and Wilson, S.K., Deformation of a Nearly Hemispherical Conducting Drop Due to an Electric Field: Theory and Experiment, *Phys. Fluids*, vol. **26**, no. 12, p. 122106, 2014.

Corson, L.T., Mottram, N.J., Duffy, B.R., and Wilson, S.K., Dynamic Response of a Thin Sessile Drop of Conductive Liquid to an Abruptly Applied or Removed Electric Field, *Phys. Rev. E*, vol. **94**, no. 4, p. 043112, 2016.

Gibbons, M.J., Howe, C.M., Di Marco, P., and Robinson, A.J., Local Heat Transfer to an Evaporating Sessile Droplet in an Electric Field, *J. Phys. Conf. Ser.*, vol. **745**, no. 3, p. 032066, 2016.

Imano, A.M. and Beroual, A., Deformation of Water Droplets on Solid Surface in Electric Field, *J. Colloid Interf. Sci.*, vol. **298**, no. 2, pp. 869–879, 2006.

Karchevsky, A.L., Marchuk, I.V., and Kabov, O.A., Calculation of the Heat Flux near the Liquid-Gas-Solid Contact Line, *Appl. Math. Modell.*, vol. **40**, no. 2, pp. 1029–1037, 2016.

Koelman, J.M.V.A., A Simple Lattice Boltzmann Scheme for Navier–Stokes Fluid Flow, *Europhys. Lett.*, vol. **15**, no. 6, pp. 603–607, 1991.

Korobeynikov, S.M., Ridel, A.V., and Medvedev, D.A., Deformation of Bubbles in Transformer Oil at the Action of Alternating Electric Field, *Europ. J. Mech. B/Fluids*, vol. **75**, pp. 105–109, 2019.

Kupershtokh, A.L., New Method of Incorporating a Body Force Term into the Lattice Boltzmann Equation, *Proc. of the 5th Int. EHD Workshop* (University of Poitiers, Poitiers, France, 2004), pp. 241–246, 2004.

Kupershtokh, A.L., Simulation of Flows with Liquid–Vapor Interfaces by the Lattice Boltzmann Method, *Vestnik NGU (Quarterly J. Novosibirsk State Univ.), Series: Math., Mech. Informatics*, vol. **5**, no. 3, pp. 29–42, 2005. (in Russian)

Kupershtokh, A.L. and Medvedev, D.A., Lattice Boltzmann Equation Method in Electrohydrodynamic Problems, *J. Electrostatics*, vol. **64**, nos. 7/9, pp. 581–585, 2006.

Kupershtokh, A.L., Medvedev, D.A., and Karpov, D.I., On Equations of State in a Lattice Boltzmann Method, *Comput. Math. Appl.*, vol. **58**, no. 5, pp. 965–974, 2009.

Kupershtokh, A.L., Criterion of Numerical Instability of Liquid State in LBE Simulations, *Comput. Math. Appl.*, vol. **59**, no. 7, pp. 2236–2245, 2010.

Kupershtokh, A.L., Ermanyuk, E.V., and Gavrilov, N.V., The Rupture of Thin Liquid Films Placed on Solid and Liquid Substrates in Gravity Body Forces, *Commun. Comput. Phys.*, vol. **17**, no. 5, pp. 1301–1319, 2015.

Kupershtokh, A.L. and Medvedev, D.A., Lattice Boltzmann Method in Hydrodynamics and Thermophysics, *J. Phys. Conf. Ser.*, vol. **1105**, p. 012058, 2018.

Kupershtokh, A.L. and Medvedev, D.A., Dynamics of Bubbles in Liquid Dielectrics under the Action of an Electric Field: Lattice–Boltzmann Method, *J. Phys. Conf. Ser.*, vol. **1359**, p. 012116, 2019.

Kupershtokh, A.L., Contact Angles in the Presence of an Electrical Field, *J. Phys. Conf. Ser.*, vol. **1675**, p. 012106, 2020.

Landau, L.D. and Lifshitz, E.M., *Electrodynamics of Continuous Media*, Oxford, UK: Pergamon Press, 1959.

Liu, Y., Oh, K., Bai, J.G., Chang, C.-L., Yeo, W., Chung, J.-H., Lee, K.-H., and Liu, W.K., Manipulation of Nanoparticles and Biomolecules by Electric Field and Surface Tension, *Comput. Methods Appl. Mech. Eng.*, vol. **197**, nos. 25-28, pp. 2156–2172, 2008.

McDonough, J.M., *Lectures on Computational Numerical Analysis of Partial Differential Equations*, Lexington, KY: University of Kentucky, 1985.

McNamara, G.R. and Zanetti, G., Use of the Boltzmann Equation to Simulate Lattice-Gas Automata, *Phys. Rev. Lett.*, vol. **61**, no. 20, pp. 2332–2335, 1988.

Medvedev, D.A. and Kupershtokh, A.L., Use of the Lattice Boltzmann Equation Method to Simulate Charge Transfer and Electrohydrodynamic Phenomena in Dielectric Liquids, *Proc. of the 2nd Int. Workshop on Conduction, Convection and Breakdown in Fluids*, Grenoble, France, pp. 60–63, 2000.

Medvedev, D.A. and Kupershtokh, A.L., Electric Control of Dielectric Droplets and Films, *Phys. Fluids*, vol. **33**, no. 12, p. 122103, 2021.

Potash, M. and Wayner, P.C., Evaporation from a Two-Dimensional Extended Meniscus, *Int. J. Heat Mass Trans.*, vol. **15**, no. 10, pp. 1851–1863, 1972.

Press, W.H., Teukolsky, S.A., Vetterling, W.T., and Flannery, B.P., *Numerical Recipes in C. The Art of Scientific Computing*, New York, NY: Cambridge University Press, 1986.

Qian, Y.H., d'Humières, D., and Lallemand, P., Lattice BGK Models for Navier–Stokes Equation, *Europhys. Lett.*, vol. **17**, pp. 479–484, 1992.

Qian, Y.H. and Chen, S., Finite Size Effect in Lattice-BGK Models, *Int. J. Mod. Phys. C*, vol. **8**, no. 4, pp. 763–771, 1997.

Shan, X. and Chen, H., Lattice Boltzmann Model for Simulating Flows with Multiple Phases and Components, *Phys. Rev. E*, vol. **47**, no. 3, pp. 1815–1819, 1993.

Taylor, G., Desintegration of Water Drops in an Electric Field, *Proc. Royal Soc. London. Ser. A Math. Phys. Sci.*, vol. **280**, no. 1382, pp. 383–397, 1964.

Vancauwenberghe, V., Di Marco, P., and Brutin, D., Wetting and Evaporation of a Sessile Drop under an External Electrical Field: A Review, *Colloids and Surfaces A: Physicochem. Eng. Aspects.*, vol. **432**, pp. 50–56, 2013.

Wang, Y., Sun, D., Zhang, A., and Yu, B., Numerical Simulation of Bubble Dynamics in the Gravitational and Uniform Electric Fields, *Numer. Heat Transf. A: Appl.*, vol. **71**, no. 10, pp. 1034–1051, 2017.

Wayner, P.C., A Dimensionless Number for the Contact Line Evaporative Heat Sink, *J. Heat Trans.*, vol. **111**, no. 3, pp. 813–815, 1989.

Zubarev, N., Self-Similar Solutions for Conic Cusps Formation at the Surface of Dielectric Liquids in Electric Field, *Phys. Rev. E*, vol. **65**, p. 055301(R), 2002.